J. Fluid Mech. (2019), *vol.* 876, *pp.* 1077–1089. © Cambridge University Press 2019
doi:10.1017/jfm.2019.563

Einstein conjecture and resting-time statistics in the bed-load transport of monodispersed particles

Luigi Fraccarollo[1],† **and Marwan A. Hassan**[2]

[1]Department of Civil, Environmental and Mechanical Engineering, University of Trento, via Mesiano, 77, 38123, Trento, Italy

[2]Department of Geography, The University of British Columbia, Vancouver, BC V6T 1Z2, Canada

(Received 22 January 2019; revised 7 July 2019; accepted 7 July 2019; first published online 14 August 2019)

Sediment transport in rivers consists, at moderate discharge stage, of individual grains that undergo a series of step movements and rest periods (bed-load). Following a large number of grain trajectories in time and space is difficult and the results are affected by bias due to censorship of the time-spatial window. Therefore, the data sets available for the description of the statistics of resting-times, travel-time and lengths of the steps, are still insufficient. In this paper, an innovative experimental methodology has been designed and applied to get data representing the evolution of a bed surface and to support a robust statistical analysis of sediment transport. The methodology is based on image sequences taken of a flat bed made of well-sorted (mono-dispersed) particles. The acquired data are interpreted analytically through equations that describe the effects of grain entrainment and deposition. We show that grains' displacement have a mean value independent of bed-load rate under low to moderate transport intensity for a given sediment type and bed-slope. Hence, we provide a strong validation of the seminal conjecture of Einstein in his theoretical statistical description of sediment transport. Finally, we describe the probability density functions of the resting-time for a few values of the sediment discharge.

Key words: sediment transport, river dynamics

1. Introduction

The transport of grains in rivers offers complex interactions among the bed surface, moving grains and water, that has continuously attracted scientists over the last century. Sediment transport on a mobile bed may take place in various conditions. We are focusing on turbulent flows at low Shields values (Shields number represents the dimensionless stress of the flow at the bed) over mild bed-slope. The transport process, under these conditions, is traditionally termed as bed-load and consists of the movement of particles that are entrained from the bed and slide, roll or jump close over it, hitting the particles at rest on the bed surface. After a number of jumps and rebounds, a particle stops in a place where it remains for a 'resting-time' interval.

† Email address for correspondence: luigi.fraccarollo@unitn.it

https://doi.org/10.1017/jfm.2019.563 Published online by Cambridge University Press

A particle movement between two successive periods of repose yields a displacement that Nikora *et al.* (2002) associated with an intermediate spatial scale. When the Shields value is high enough, a dense sub-layer of moving grains forms in the lower part of the flow (Capart & Fraccarollo 2011), and the particles rarely stay at rest, sustained by their own collisions (collisionally suspended sediment transport). This can happen also in laminar flows (Ouriemi, Aussillous & Guazzelli 2009). However, the statistics of resting-times and displacements are meaningful only under bed-load conditions. For mono-dispersed bed mixtures, Einstein (1950) proposed the following law to express q_s, the volumetric sediment discharge per unit of width

$$q_s = ELV_p, \tag{1.1}$$

based on statistical predictors E, the mean number of particles entrained per unit of bed surface and per unit of time, and L, the mean travel distance run by particles between two subsequent rests. V_p is the representative particle volume. Applying (1.1) requires the determination of E and L as functions of flow and bed conditions. Einstein's basic conjecture is that L is proportional to the grain size, independent of the transport stage, in the bed-load regime. Following Einstein (1950), several models based on a probabilistic description of the bed-load process have been proposed (Paintal 1971; Nikora *et al.* 2002; Ancey *et al.* 2006; Lajeunesse, Malverti & Charru 2010; Fan *et al.* 2014; Fathel, Furbish & Schmeeckle 2015). Statistical results involving the measurement of local bed-elevation fluctuations in flume experiments suggest that resting-times follow power law distributions associated with long-term sub-diffusive transport while, over longer timescales, they are best described by an exponential distribution (Voepel, Schumer & Hassan 2013). Travel distances and resting-times are strongly affected by morphological units, such as pools, bars and dunes, which superimpose their transport characteristics (Habersack 2001; Pyrce & Ashmore 2003; Kasprak *et al.* 2015; Hassan & Bradley 2017). Critical issues to the predictive development proposed by Einstein of (1.1) come from either the proposition of probability distributions without characteristic spatial scales (Ancey *et al.* 2006; Ganti *et al.* 2010; Hill, DellAngelo & Meerschaert 2010; Campagnol *et al.* 2013) or from how it deals with particle velocity, resting-time, transition from low to high transport stages, and solid-discharge fluctuation distributions (Ancey *et al.* 2006). An important body of research aiming at evaluating entrainment and deposition rates under general flow conditions has recently developed (see Seminara, Solari & Parker 2002; Charru, Mouilleron & Eiff 2004; Lajeunesse *et al.* 2010). This effort permits supplying phenomenological closures for the predictors of (1.1) (or similar) and to make it, eventually, a predictive tool. This work does cover this fundamental issue. To get reliable estimates of the transport predictors in (1.1), the natural approach consists of tracking the trajectories of a large number of grains to obtain information on both step lengths and rest periods (Habersack 2001; Nikora *et al.* 2002; McNamara & Borden 2004; Ancey *et al.* 2006; Campagnol *et al.* 2013). Particle-tracking techniques are usually affected by technical limitations and offer, at most, only hundreds of trajectories, which are semi-automatically reconstructed (Campagnol *et al.* 2013). Seizilles *et al.* (2014) were able to follow up to approximately 10 000 particle trajectories in a laminar flow, chiefly focusing on lateral transport. Bed-load trajectories referring to poorly sorted sediment-size mixtures and/or to the presence of bed forms, though the expected strong effects of these features on the results, are still not documented in experimental works. To confirm the importance and the need of further experimental analyses on bed-load, a recent paper of Ballio

https://doi.org/10.1017/jfm.2019.563 Published online by Cambridge University Press

Runs	1	2	3	4	5	6	7	8	9
$\tilde{q}_s$ (−)	0.014	0.16	0.035	0.042	0.086	0.089	0.14	0.16	0.20
$\tilde{t}_\infty$ (−)	4.0×10^5	3.3×10^5	1.3×10^5	1.2×10^5	5.0×10^4	4.6×10^4	1.6×10^4	3.3×10^3	8.3×10^2

TABLE 1. Bed-load rate, $\tilde{q}_s$ and $\tilde{t}_\infty$, the dimensionless time needed to reach an almost complete substitution of the pristine particles, for the nine runs.

et al. (2018) bridges Lagrangian and Eulerian outcomes, clarifying limitations of the laboratory set-up with respect to the different reference frames, and enabling operational solutions to be applied.

In contrast with all previous experimental analyses, we provide statistical information on grain movements not based on trajectory reconstruction, but on a straightforward and continuous gauge of the tone of any pixel within a large image sequence. Our procedure is equivalent to obtaining thousands of trajectories and is fully automated, without operator checks and censorship due to the limited sizes of a spatial-temporal observation window (see Ballio *et al.* 2019), allowing us to reach an unprecedented precision in the description of the entrainment process.

2. Experimental set-up, run and measurement description

Nine experimental runs were conducted in a 10 cm wide and 6 m long recirculating flume at DICAM, University of Trento, Italy. In each run, sediment and water discharges were constant, and the flow was uniform. Low bed-slopes i_b were set in all runs (approximately 0.3°–0.5°). The mobile bed consisted of well-sorted (in size and shape) PVC pseudo-cylindrical grains of equivalent spherical diameter $d = 3.24 \pm 0.08$ mm (mean $\pm$ standard deviation). The specific submerged density of the particles was $\Delta = \rho_s/\rho_w - 1 = 0.51$, where ρ_s and ρ_w are the mass densities of grains and water, respectively. Fall velocity of the particles was approximately $w = 0.18$ m s^{-1} and their critical angle of internal friction $\alpha = 31°$, measured at very slow shear rates. Most of the grains are white, some are grey, some black. The runs present flow depths h between 2–3 cm and flow discharges between 5 and 15 l m s^{-1}. No direct measurements of the flow velocity have been performed.

Variables and results will be reported in dimensionless terms. The dimensionless variables will be denoted by the $\tilde{\cdot}$ accent. Our choice is to make times and distances dimensionless by division with, respectively, $\sqrt{d/\Delta g}$ and by d, where g is the gravitational acceleration. In dimensionless terms, equation (1.1) becomes

$$\tilde{q}_s = \tilde{E}\tilde{L}\tilde{V}_p, \quad \text{where } \tilde{q}_s = \frac{q_s}{\sqrt{g\Delta d^3}}, \quad \tilde{E} = E\sqrt{\frac{d^5}{g\Delta}}, \quad \tilde{L} = \frac{L}{d}, \quad \text{and} \quad \tilde{V}_p = \frac{V_p}{d^3} \approx \frac{1}{2}. \tag{2.1}$$

Some dimensionless run data are reported in table 1. The recirculated sediment discharge $\tilde{q}_s$ varied, from run to run, over the range 0.014–0.200 (−). The dimensionless value of the sediment discharge, not the Shields stress $\tilde{\Theta} = hi_b/(\Delta d)$, has been chosen as the reference value to feature the run condition. Though a direct measurement of the Shields stress is available, it is expected to be inaccurate. In fact, it requires measuring the flow depth h and the bed-slope i_b. The flow depth is oscillating a few millimetres in space and time, while the slope is small and its measurement is coarse, affected by errors on even the first digit. On the contrary, the sediment discharge (and

https://doi.org/10.1017/jfm.2019.563 Published online by Cambridge University Press

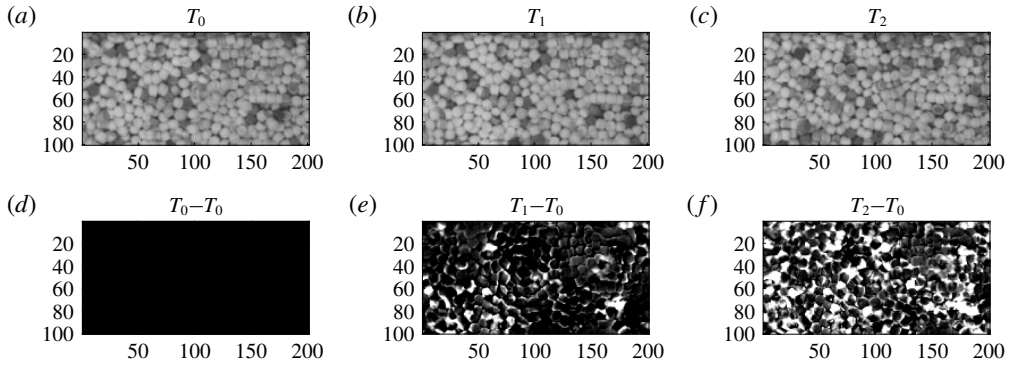


FIGURE 1. (*a–c*) Time sequence of three real images, taken at the times T_i, $i = 0, 1, 2$ increasing with the subscript. (*d–f*) Images obtained after subtracting the first image, taken at T_0, from the real images of the top row. Units along both axes are dimensionless distances (x and y divided by d).

the flow discharge, too), measured through volumetric sampling for long time at the outlet of the flume, showed up to be accurate and steady (oscillation within a few % units). To complete the presentation of the hydraulic parameters, calling U the average flow velocity and ν the water kinematic viscosity, we report that the Froude number ($Fr = U/\sqrt{gh}$) in the various runs varied approximately between 0.4 and 0.6 (−), the Reynolds number ($Re = Uh/\nu$) approximately between 3×10^3 and 13×10^3 (−) and the particle Reynolds number ($Re_p = \sqrt{g\Delta d}/\nu$) was approximately 400 (−).

A video camera positioned approximately 1 m above the free surface was used to record images of the bed surface during the run. Each image covers a bed surface area (BSA) of approximately 9×35 cm^2, consisting of roughly 3–4 $\times 10^3$ visible grains. Lighting is an important issue. We used two sources of diffused, not flickering, LED lights, which illuminated the bed surface through the transparent sidewall. The lighting is free from outside biases, as the entire flume was covered by a single piece of thick cloth. The recorded images are frames measuring 1024 pixel × 256 pixel, acquired as matrices having the numbers of rows and columns equal to the sizes, in pixel units, of the image. Figure 1(*a–c*) shows a portion of the acquired images at three subsequent instants T_0, T_1, T_2. The resolution of the images is high enough to allow us to see and identify the particles lying on the bed surface. A single particle occupies up to 100 pixels. Figure 1(*d–f*) shows a sequence of special images obtained after subtracting the T_0 image from the real images (see (2.3)). This technique has already been used for other purposes (Heays, Friedrich & Melville 2014) and is termed 'digital erosion'. The subtraction allows us to assess whether or not any pixel in the current image is occupied by the same grain or group of grains already present in the first image. The particles viewed in the BSA in the first image, at T_0, are important in our analysis, and will be referred to as 'pristine'. They form the statistical sample of the present analysis.

We worked through the recorded images of the BSA (figure 1*a–c*). Herein, the underscript ∞ refers to values of quantities at a time equal to, or later than, $\tilde{t}_\infty$, (see table 1), a finite time value after which the asymptotic entrainment of all the pristine particles has ended. First, we calculated the dimensionless chromatic area, $\tilde{a}(\tilde{t})$, defined as

$$\tilde{a}(\tilde{t}) = \frac{a(\tilde{t})}{a_\infty}, \tag{2.2}$$

https://doi.org/10.1017/jfm.2019.563 Published online by Cambridge University Press

where $a(\tilde{t})$ and a_∞ are

$$a(\tilde{t}) = \sum_{i=1}^{N}\sum_{j=1}^{M} |A_{ij}(\tilde{t}) - A_{ij}(0)|; \quad a_\infty = a(\tilde{t}_\infty), \tag{2.3a,b}$$

with N and M being the dimensions of the frame matrix; subscripts i, j represent the pixel position in the image-frame (i.e., a matrix) $\boldsymbol{A}$. The matrix entries A_{ij} represent the grade in the grey-scale range (integer values from 0 to 255) of the pixel at position i, j of the real image-frame taken at time t. The acquired images are standard 'bmp' files. To convert them into a matrix, we used MATLAB ('imread' function). At $\tilde{t} = 0$, the first image (the pristine one) is taken, $A_{ij}(\tilde{t})$ are the pixel tones of an image-frame taken at the current time $\tilde{t}$; $A_{ij}(\tilde{t}_\infty)$ are the pixel tones of an image-frame taken at a later time ($\tilde{t} \geqslant \tilde{t}_\infty$), being the asymptotic times $\tilde{t}_\infty$ reported in table 1.

Any entrainment or deposition of a grain yields variations of the grey-scale grade in the image pixels occupied by that grain (approximately 100 pixels on average per fully visible grain). Entrainment of non-pristine particles lying over non-pristine particles, or deposition of an incoming particle over non-pristine parts of the BSA, provokes local changes of the pixel tones, but no changes on the global function $\tilde{a}(\tilde{t})$. Only the entrainment of pristine particles provokes a steady change of $\tilde{a}(\tilde{t})$. Burial and reappearance of a pristine particle has also substantial effects on $\tilde{a}(\tilde{t})$, but they cancel out as time passes. As time increases after the start of the run, the subtracted images (figure 1*d–f*) change from being all black (grey level = 0) to becoming images with pixel tones in the whole grey range 0–255 (like any original image in the top row of the figure). The function $a(\tilde{t})$ (2.3), tells us how many pristine particles, over their total number, are not visible at time $\tilde{t}$, and is changing from 0 toward its horizontal asymptote. Then, from (2.2), $\tilde{a}(\tilde{t})$ is a function starting from 0, at $\tilde{t} = 0$, and moving around $\tilde{a} = 1$, at $\tilde{t} \geqslant \tilde{t}_\infty$. The increase of $\tilde{a}$, from 0 to 1 is not necessarily strictly monotonic. After $\tilde{t}_\infty$ the pristine bed surface has been almost completely rearranged, i.e., no more pristine particles are still in the place they were at $\tilde{t} = 0$. Such a condition is supported by visual inspections of the images and by the function $\tilde{a}(\tilde{t})$ asymptotically tending to unity.

The moving particles that appear in the first image are not pristine and move away soon, causing an abrupt increase of the modified area function at the start of the process. This discontinuous jump of $a(t)$, which is smaller in the runs with lower sediment discharge, must be subtracted from the $a(t)$ values, so that the modified area function starts from zero. Other temporary changes are due to moving grains passing over the BSA, without stopping on it, or to free-surface wrinkling; these processes alter some spots, but only momentarily, producing meaningless small and quite short fluctuations in the output. These are filtered out by fitting the measured modified areas with analytic functions.

A key assumption we make is that the way $\tilde{a}(\tilde{t})$ evolves, from 0 to the asymptote 1, represents the percentage of the pristine particles that are either presently covered (at time $\tilde{t}$) or that have been already entrained (before time $\tilde{t}$). Since we are measuring colour tones and do not directly count the pristine particles, the assumption needed to be validated. It has been easily and fully satisfactorily checked by using a stochastic model. Figure 2 shows some relevant results.

In figure 3(*a*), we present the evolution of the chromatic area $\tilde{a}(\tilde{t})$ for four runs. The time window is limited to a few hundred dimensionless time units, thus it may not be evident that all the curves actually tend toward unity. The lower the value of $\tilde{q}_s$, the higher the value of $\tilde{t}_\infty$ (table 1). We repeated most of the runs a few times in

https://doi.org/10.1017/jfm.2019.563 Published online by Cambridge University Press

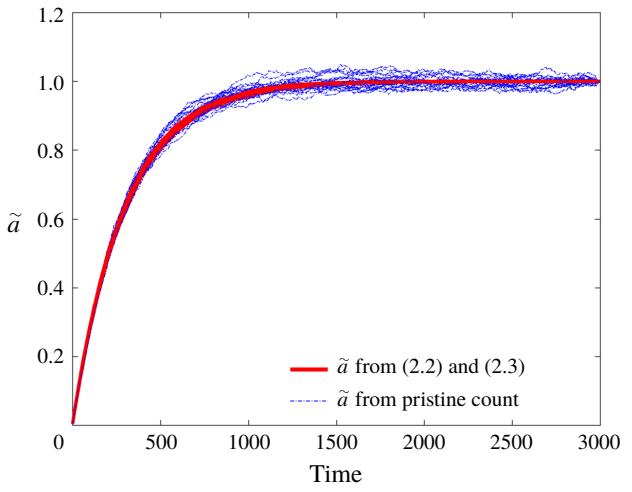


FIGURE 2. (Colour online) Values of $\tilde{a}(\tilde{t})$ of an artificial image made of $N_t = 3000$ pixels (approximately the number of particles we have in a real image), evolved by randomly substituting, at any time unit, the colour tone of 100 pixels. We calculated $\tilde{a}(\tilde{t})$ either by using (2.2)–(2.3) or by counting the number of pristine pixels N_p at any time and used it as the input in the following expression $\tilde{a}(\tilde{t}) = 1 - N_p(\tilde{t})/N_t$. We report 20 realisations of the stochastic process.

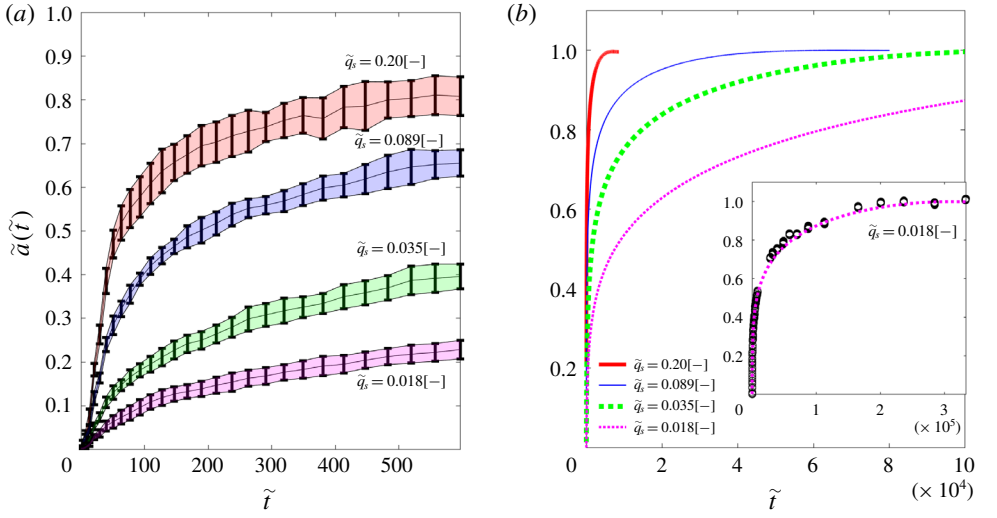


FIGURE 3. (Colour online) (*a*) Experimental evolution of $\tilde{a}(\tilde{t})$ for four experimental runs, tagged with the relevant values of $\tilde{q}_s$ The solid lines connect the mean values obtained from several repetitions, the shaded areas envelop the interval bars. (*b*) Curves representing the analytic fitting of $\tilde{a}(\tilde{t})$, for the same runs of (*a*), for a longer time interval. The curves stop when the asymptote $\tilde{a}(\tilde{t}) = 1$ is reached. In the inset the fitting curve along with the experimental data (circles) for a single realisation of run $\tilde{q}_s = 0.018$ (−).

order to get a mean value and an interval bar at any time of their evolution. For the same runs and longer times, figure 3(*b*) shows the analytic functions fitting the $\tilde{a}(\tilde{t})$ measurements, with an inset devoted to the slowest run, where all the measurements for a single realisation and the fitting curve are displayed together.

https://doi.org/10.1017/jfm.2019.563 Published online by Cambridge University Press

3. Theoretical analysis

Any particle lying on the bed surface is endowed with a stochastic property, the resting-time $\tilde{T}_r$, i.e., the time interval (a positive quantity) from its last arrest to its next entrainment. Despite their similarity in all aspects (shape, size, density, etc.), the grains on the bed surface have a different probability of being entrained, reflecting different responses to near-bed fluid turbulence. Different values of $\tilde{T}_r$ mirror different stability of the grains due to local (at the grain scale) packing, imbrication or flow conditions. Once a particle is entrained, it loses any link to its former condition; when it stops on the bed again, it gains a new value of $\tilde{T}_r$, and so on. We assumed that the resting-times associated with the grains on the BSA form a statistical population. Hereafter we describe the theoretical approach that exploits the measured chromatic area $\tilde{a}(\tilde{t})$ to get, or approximate, the probability density function $p(\tilde{T}_r)$ of the resting-times. The statistical mean of its inverse, $\langle \tilde{T}_r^{-1} \rangle$, is the mean entrainment frequency of the grains on the bed surface. According to the definition of $\tilde{E}$, in (2.1), $\langle \tilde{T}_r^{-1} \rangle$ is equal to the product of $\tilde{E}$ and a particle shape coefficient, that represents the average bed-surface area occupied by a single particle, divided by d^2 and by the volumetric sediment-concentration of the static bed. This coefficient is close to 1 for both closely packed spheres or for uniformly-oriented and aligned cubes, hence it is assumed

$$\langle \tilde{T}_r^{-1} \rangle \approx \tilde{E}. \tag{3.1}$$

The start of the recording, when the first image is taken, is chosen to be $\tilde{t} = 0$, where $\tilde{t}$ is the current time of the evolution process. In a single run, the evolution of the chromatic area $\tilde{a}(\tilde{t})$ is modelled through the following equation

$$\frac{\mathrm{d}\tilde{a}}{\mathrm{d}\tilde{t}}(\tilde{t}) = \underbrace{p_c(\tilde{t})}_{Pr.Entr.Act} + \underbrace{\langle \tilde{T}_r^{-1} \rangle (1 - \tilde{a})}_{Pr.Bur.Act} - \underbrace{\langle \tilde{T}_r^{-1} \rangle \int_0^{\tilde{t}} (1 - \tilde{a}(\xi)) p(\tilde{t} - \xi)\, \mathrm{d}\xi}_{Pr.Reap.Act}, \tag{3.2}$$

where p_c is the probability density function (p.d.f.) of the censored resting-times $\tilde{T}_c$, i.e, the resting-time interval of the pristine particles calculated from time $\tilde{t} = 0$ and not from the actual inlet time $\tilde{t}_i \leqslant 0$, at which the pristine particle reached its position in the BSA. Because the pristine particles have already been sitting for some time in the position that they occupy at $\tilde{t} = 0$, $\tilde{T}_r = \tilde{T}_c - \tilde{t}_i \geqslant \tilde{T}_c \geqslant 0$ holds. Here ξ is a dummy variable for time in the convolution term.

Equation (3.2) is a kind of conservation equation for the exposed surface of the pristine particles that governs the modification of the pixel values of the BSA. Under uniform and steady flow conditions and a flat bed, entrainment and deposition even out at any time, and both contribute to modify the chromatic area. Specifically, three acts affect, during the run, the value of $\tilde{a}(\tilde{t})$. First, when a pristine particle is entrained, a random change occurs in the grey-tone of the pixels occupied by that particle. This is referred to as 'pristine entrainment act'. Second, a particle coming from upstream can arrive and settle in a position over the BSA. If such a particle covers in part or totally pristine particles, then a temporary change of the grey-tone of the corresponding local pixels takes place. This is referred to as 'pristine burial act'. Third, when this particle will be later entrained, after even a long residence period, the image of the local pristine bed will be restored. This act will be referred to as 'pristine reappearance act'. These three acts are mathematically represented in the three terms in the right-hand

https://doi.org/10.1017/jfm.2019.563 Published online by Cambridge University Press

side of (3.2) and are responsible of the monotonic increment of $\tilde{a}(\tilde{t})$ from 0 to 1. The 'pristine entrainment act' and the 'pristine burial act' terms are always positive and are summed; the last term refers to the 'pristine reappearance act' and is positive, but is subtracted. The 'pristine burial act' term is proportional to $(1-\tilde{a})$ because we assumed that the conditional probability for an arriving particle to stop in the BSA over a pristine (or non-pristine) particle is only equal to the fraction of bed occupied by pristine (or non-pristine) particles. Last contribution ('pristine reappearance act') is a convolution integral that involves the distribution $p(\tilde{T}_r)$. Here we assumed that the probability density function of the resting-times of the arriving, non-pristine, particles, once they deposit, is identical to the $p(\tilde{T}_r)$ of the pristine particles occupying the bed at $\tilde{t}=0$. This term starts from zero, at $\tilde{t}=0$, and ends at zero, at $\tilde{t}\geqslant\tilde{t}_\infty$, when no pristine particles may be found and hidden anymore. The integral over time, from 0 to ∞, of the difference between the 'pristine burial act' term and the 'pristine reappearance act' term is null, as can be easily proved by using the Fubini theorem. Hence, from (3.2), $\int_0^\infty p_c\,\mathrm{d}\xi=\tilde{a}(\infty)-\tilde{a}(0)=1$, as expected for a probability density function.

Another relation between $p(\tilde{T}_r)$ and $p_c(\tilde{T}_c)$ can be established by considering that the inlet time, $\tilde{t}_i$, is also a stochastic variable, fully uncorrelated to $\tilde{T}_r$. A pristine particle has an equally distributed probability to have entered the BSA in the time interval $[-\tilde{T}_r, 0]$, with $\tilde{T}_r$ being its resting-time. Hence, the contribution to $p_c(\tilde{T}_c)$ from pristine particles having resting-time $\tilde{T}_r$, is proportional to $p(\tilde{T}_r)$ itself, and inversely proportional to $\tilde{T}_r$. Keeping in mind that, at any $\tilde{t}\geqslant 0$, only pristine particles having $\tilde{T}_r\geqslant\tilde{t}$ are still sitting in the BSA, the censored-time p.d.f., $p_c(\tilde{T}_c)$, is built over just a part of the resting-time p.d.f., $p(\tilde{T}_r)$, that is over $p(\tilde{T}_r\geqslant\tilde{T}_c)$. Therefore, stringing all these concepts together, the following expression holds

$$p_c(\tilde{T}_c)=\int_{\tilde{T}_c}^{\infty}\frac{p(\xi)}{\xi}\,\mathrm{d}\xi, \tag{3.3}$$

where ξ is a dummy variable for resting-time. Through the Fubini theorem again, it is straightforward to check that $\int_0^\infty p\,\mathrm{d}\xi=1$, as it must be for a probability density function. From taking the derivative with respect to $\tilde{T}_c$ of both sides of (3.3), the result is

$$p(\tilde{T}_r)=-\tilde{T}_c\frac{\mathrm{d}p_c(\tilde{T}_c)}{\mathrm{d}\tilde{T}_c},\quad \text{at } \tilde{T}_c=\tilde{T}_r. \tag{3.4}$$

Equations (3.2) and (3.4) form a coupled system in the unknown probability density functions, that is $p(\tilde{T}_r)$ and $p_c(\tilde{T}_c)$. Of course, as the motion is steady uniform, the solutions do not depend on the starting time $\tilde{t}=0$, nor on the choice of the BSA location. In solving (3.2) and (3.4), we replaced the measured chromatic area $\tilde{a}(\tilde{t})$ with its fitted analytic function. Its time derivative was then used in (3.2) within the range $0\leqslant\tilde{a}\leqslant 0.99$.

We can further show that $p_c(0)$ is equal to $\langle\tilde{T}_r^{-1}\rangle$, and, in turn, equal to $\tilde{E}$ (3.1). To show this, let us build the p.d.f. of the variable $\langle\tilde{T}_r^{-1}\rangle$: it, being the inverse of the resting-time, has a p.d.f. equal to $p(\tilde{T}_r)\tilde{T}_r^2$; by definition, its mean is

$$\langle\tilde{T}_r^{-1}\rangle=\int_\infty^0[p(\xi)\xi^2]\frac{1}{\xi}\,\mathrm{d}\left(\frac{1}{\xi}\right)=\int_0^\infty\frac{p(\xi)}{\xi}\,\mathrm{d}\xi. \tag{3.5}$$

https://doi.org/10.1017/jfm.2019.563 Published online by Cambridge University Press

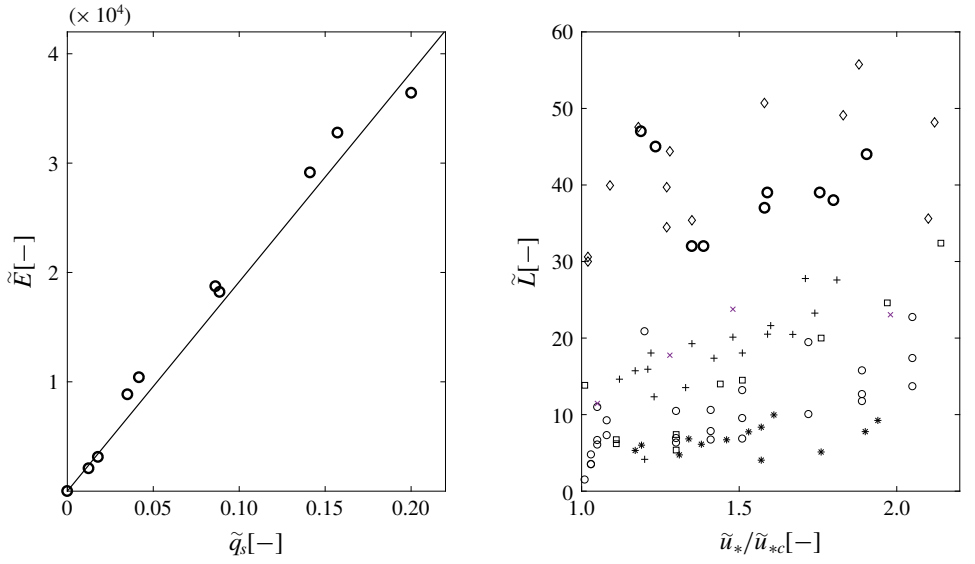


FIGURE 4. (*a*) Linear fitting between $\tilde{E}$ and $\tilde{q}_s$; bold circles represent the measurements. (*b*) Values of $\tilde{L}$ from our measurement (bold circles) and from other authors (from figure 5 of Campagnol, Radice & Ballio (2012)), versus the ratio between friction velocity and its critical value.

Then, from (3.3)

$$\int_0^\infty \frac{p(\xi)}{\xi}\,\mathrm{d}\xi = p_c(0). \tag{3.6}$$

This information is important, as it represents a constraint, which must be satisfied in solving the system of (3.2) and (3.4).

More important, from (3.2), evaluated at $\tilde{t}=0$, (3.5) and (3.6) it can be inferred that $\langle \tilde{T}_r^{-1} \rangle$ is readily available (and so is predictor $\tilde{E}$ through (3.1)) from the derivative of $\tilde{a}(\tilde{t})$ at $\tilde{t}=0$

$$\langle \tilde{T}_r^{-1} \rangle = p_c(0) = \frac{1}{2}\frac{\mathrm{d}\tilde{a}}{\mathrm{d}\tilde{t}}(\tilde{t}=0). \tag{3.7}$$

4. Results

From the evolution of the chromatic area, we may directly extract both the predictors $\tilde{E}$ and $\tilde{L}$ of the sediment discharge relation (2.1). The term $\tilde{E}$ comes from (3.7). Figure 4(*a*) reports the obtained values of $\tilde{E}$ versus $\tilde{q}_s$; they appear to vary in a proportional way. Their relation is fitted with the line defined in following equation (4.1), crossing the origin and having a R^2 regression coefficient equal to approximately 0.98

$$\tilde{E} = \beta \tilde{q}_s, \quad \text{with } \beta = 0.050\,(-). \tag{4.1}$$

With this, we move to find the other predictor, $\tilde{L}$ (see (2.1)). It is simple to substitute $\tilde{E}$ with the right-hand side of relation (4.1) into $\tilde{q}_s = \tilde{E}\tilde{L}\tilde{V}_p$ (2.1), to get

$$\tilde{L} \approx 40\,(-). \tag{4.2}$$

https://doi.org/10.1017/jfm.2019.563 Published online by Cambridge University Press

In comparison, Einstein (1950) proposed $\tilde{L} \approx 100$ (−). This value is still a mean value that corresponds to a probability distribution function for the travel distances. The reconstruction of this p.d.f. remains an open issue in the present work. The quality and extension of the presented data provide a neat support to Einstein's seminal assumption about the independence of $\tilde{L}$ on sediment discharge $\tilde{q}_s$ (and therefore on Shields) in the ordinary bed-load regime and when the bed is formed by given mono-dispersed sediments. Previous experimental research based on the use of tracking techniques and conducted at low Shields stress values (Drake *et al.* 1988; Niño & Garcia 1996; Séchet & Le Guennec 1999; Lee *et al.* 2006; Lajeunesse *et al.* 2010; Martin, Jerolmack & Schumer 2012; Campagnol *et al.* 2013) yielded $\tilde{L}$ values ranging between 1 and 100 (−). In some of these studies, it was also suggested, in contrast with our results, that the dimensionless travel distance depends on the transport stage, either through a power law (Lee *et al.* 2006) or a linear relation (Lajeunesse *et al.* 2010). In figure 4(*b*) we plotted the values of $\tilde{L}$ versus the ratio of the dimensionless friction velocity $\tilde{u}_*$ and its critical value $\tilde{u}_{*,c} = \sqrt{\tilde{\Theta}_c}$, presented by various authors (most are cited above) and found in figure 5 of Campagnol *et al.* (2012). Here $\tilde{\Theta}_c$ is the critical Shields value at the threshold of particle motion (Pähtz & Durán 2018), here assumed equal to 0.05, close to the threshold value of the Meyer-Peter and Müller equation and within the range reported in Shields diagram (Shields 1936). To express the friction velocity we did not rely on our measurements of flow depth h and bed-slope i_b, for the accuracy reasons already reported. Instead, we used the Meyer-Peter and Müller equation as a tool to get the $\tilde{u}_*$ value from the measured sediment discharge. In fact, according to the Meyer-Peter and Müller equation (Wong & Parker 2006), it holds that

$$\tilde{u}_*^2 = \tilde{\Theta}_c + (\tilde{q}_s/4)^{2/3}. \tag{4.3}$$

Spanning over a limited range of $\tilde{u}_*/\tilde{u}_{*,c}$, figure 4(*b*) shows that our measured values of $\tilde{L}$ oscillates with no apparent trend around their mean with a standard deviation of approximately 5 (−). This result supports a constant $\tilde{L}$ but says nothing about what $\tilde{L}$ would be for other particle type and size or its dependence on the bed-slope and flow regime (laminar, turbulent). Indeed, the scattering of data from various authors shown in figure 4(*b*) indicates that the Einstein assumption is not exhaustive in describing the travelling process in all conditions, and the need for further research in this area is still needed.

Up to here, our findings join previous results, agreeing or not, from flume or field data, though obtained through an original methodology. What is novel here is the provision of $p(\tilde{T}_r)$ and the way we obtained it, which is analytic (once the images are available) and not based on direct measurements of $\tilde{T}_r$ that imply (so far) technical troubles. To get the probability distribution of the resting-times, we had to solve (3.2) and (3.4) for the two probability density function's unknowns, p and p_c, having, as experimental input, the function $\tilde{a}(\tilde{t})$. We developed the solution for the four runs already considered in figure 3. The numerical results for $p(\tilde{T}_r)$, pursued through a recursive trial and error approach, are reported in figure 5(*a*), where both axes are logarithmic. We checked that the obtained $p(\tilde{T}_r)$ satisfy all the constraints, i.e., to be positive with a unit integral, and to provide a mean of $\langle \tilde{T}_r^{-1} \rangle$ from (3.5) coinciding with the value from (3.7). In figure 5(*a*) each curve is tagged in the legend by the relevant values of $\tilde{q}_s$ and $\langle \tilde{T}_r \rangle$. At a first sight the four $p(\tilde{T}_r)$ curves display long and linear tails, in the log–log plots, features in common with power-law

https://doi.org/10.1017/jfm.2019.563 Published online by Cambridge University Press

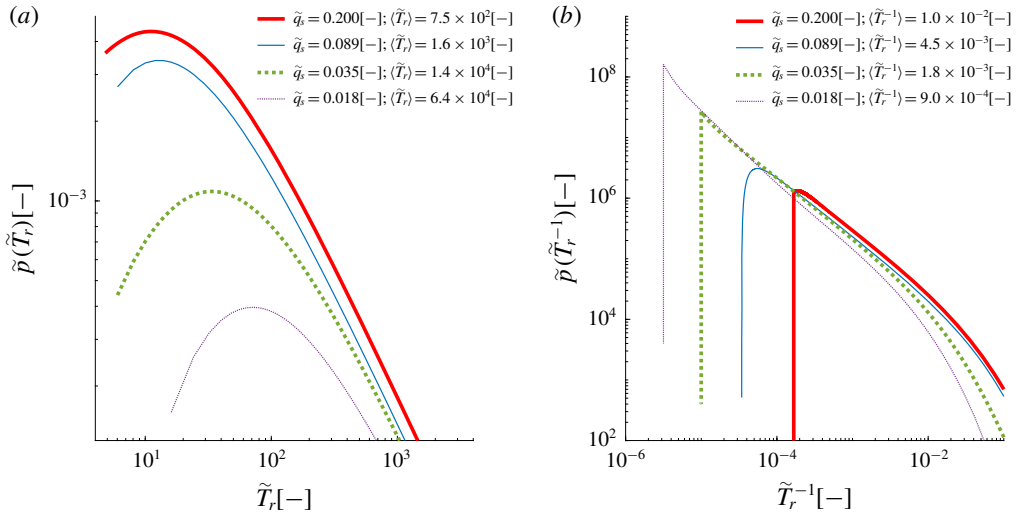


FIGURE 5. (Colour online) (*a*) Probability density functions $p(\tilde{T}_r)$ for four runs, identified by the values of $\tilde{q}_s$ and $\langle \tilde{T}_r \rangle$. (*b*) Probability density functions $p(\tilde{T}_r^{-1})$ for four runs, identified by the values of $\tilde{q}_s$ and $\langle \tilde{T}_r^{-1} \rangle$.

distributions (Voepel *et al.* 2013). The mean resting-time decreases hyperbolically as $\tilde{q}_s$ increases. By increasing $\tilde{q}_s$ beyond the values featuring the nine performed runs, it would be approached the boundary between ordinary and collisionally suspended bed-load (Berzi & Fraccarollo 2013). This latter, intense sediment-transport regime is associated with the formation of an almost full layer of moving grains, which undergo mutual collisions and have little, almost null, rest-time. Hence, the Einstein conjecture, which applies to ordinary bed-load, breaks when the power of the stream is high enough to make the collisions between moving grains a dominant mechanism of the transport process.

Figure 5(*b*) displays the probability density functions $p(\tilde{T}_r^{-1})$ for the four runs of (*a*), identified now by the values of $\tilde{q}_s$ and $\langle \tilde{T}_r^{-1} \rangle$. The two panels of figure 5, together, provide a description of how the resting-times are distributed at the extremes, when $\tilde{T}_r$ tends to either 0 or ∞.

5. Conclusions

Statistical information for ordinary bed-load transport have been obtained through an innovative experimental methodology based on image analysis applied where the bed is flat and made of well sorted particles. Two major findings are presented. The first one is a robust confirmation of Einstein's assumption about average grain displacement, the distance run between two subsequent resting periods, which is shown to scale with only the grain-size at a given bed-slope. The second achievement consists of the probability density function of the grain resting-time inferred through a theoretical analysis of the raw data. These outcomes may be exploited in mechanical/statistical interpretation of the ordinary bed-load process or in the determination of associated features, e.g., the dispersion of pollution carried by the grains. Future analysis could address the role of the grain shape and of the bed-slope to see how our results can be extended to more general conditions.

https://doi.org/10.1017/jfm.2019.563 Published online by Cambridge University Press

Acknowledgements

The authors thank the associate editor, E. Guazzelli, and the anonymous reviewers for their commitment and guidance. The experiments have been performed with the vital help of two students, now engineers, A. Viviani and M. Verber. The technicians of the Hydraulic Laboratory of the University of Trento (A. Bampi, L. Forti, F. Sartori and P. Scarfiello) have, as always, provided the best setting to perform experimental works. K. Wlodarczyk (UBC, Vancouver) gave a generous English revision. Fruitful discussions have been had by the authors, at different stages of the work, with F. Ballio, D. Berzi, J. Campagnol, P. Frey, D. Furbish, J. Heyman, M. Larcher, S. Siboni and A. Radice.

REFERENCES

ANCEY, C., BÖHM, T., JODEAU, M. & FREY, P. 2006 Statistical description of sediment transport experiments. *Phys. Rev.* E **74** (1), 011302.

BALLIO, F., POKRAJAC, D., RADICE, A. & SADABADI, S. A. H. 2018 Lagrangian and Eulerian description of bed load transport. *J. Geophys. Res.: Earth Surface* **123** (2), 384–408.

BALLIO, F., RADICE, A., FATHEL, S. L. & FURBISH, D. J. 2019 Experimental censorship of bed load particle motions, and bias correction of the associated frequency distributions. *J. Geophys. Res.* **124** (1), 116–136.

BERZI, D. & FRACCAROLLO, L. 2013 Inclined, collisional sediment transport. *Phys. Fluids* **25** (10), 106601.

CAMPAGNOL, J., RADICE, A. & BALLIO, F. 2012 Insight on how bed configuration affects properties of bed load motion. In *Proceedings of the 6th International Conference on Scour and Erosion (ICSE-6), Paris, France* (ed. J.-J. Fry & C. Chevalier), pp. 27–34. Société Hydrotechnique De France.

CAMPAGNOL, J., RADICE, A., NOKES, R., BULANKINA, V., LESCOVA, A. & BALLIO, F. 2013 Lagrangian analysis of bed-load sediment motion: database contribution. *J. Hydraul Res.* **51** (5), 589–596.

CAPART, H. & FRACCAROLLO, L. 2011 Transport layer structure in intense bed-load. *Geophys. Res. Lett.* **38** (20), L20402.

CHARRU, F., MOUILLERON, H. & EIFF, O. 2004 Erosion and deposition of particles on a bed sheared by a viscous flow. *J. Fluid Mech.* **519**, 55–80.

DRAKE, T. G., SHREVE, R. L., DIETRICH, W. E., WHITING, P. J. & LEOPOLD, L. B. 1988 Bedload transport of fine gravel observed by motion-picture photography. *J. Fluid Mech.* **192**, 193–217.

EINSTEIN, H. A. 1950 *The Bed-Load Function for Sediment Transportation in Open Channel Flows*, vol. 1026. US Department of Agriculture.

FAN, N., ZHONG, D., WU, B., FOUFOULA-GEORGIOU, E. & GUALA, M. 2014 A mechanistic-stochastic formulation of bed load particle motions: from individual particle forces to the Fokker–Planck equation under low transport rates. *J. Geophys. Res.* **119** (3), 464–482.

FATHEL, S. L., FURBISH, D. J. & SCHMEECKLE, M. W. 2015 Experimental evidence of statistical ensemble behavior in bed load sediment transport. *J. Geophys. Res.* **120** (11), 2298–2317.

GANTI, V., MEERSCHAERT, M. M., FOUFOULA-GEORGIOU, E., VIPARELLI, E. & PARKER, G. 2010 Normal and anomalous diffusion of gravel tracer particles in rivers. *J. Geophys. Res.* **115** (F2), F00A12.

HABERSACK, H. M. 2001 Radio-tracking gravel particles in a large braided river in New Zealand: a field test of the stochastic theory of bed load transport proposed by Einstein. *Hydrol. Process.* **15** (3), 377–391.

HASSAN, M. A. & BRADLEY, D. N. 2017 Geomorphic controls on tracer particle dispersion in gravel bed rivers. In *Gravel-Bed Rivers: Process and Disasters* (ed. D. Tsutsumi & J. B. Laronne), chap. 6, pp. 159–184. Wiley-Blackwell.

https://doi.org/10.1017/jfm.2019.563 Published online by Cambridge University Press

HEAYS, K. G., FRIEDRICH, H. & MELVILLE, B. W. 2014 Laboratory study of gravel-bed cluster formation and disintegration. *Water Resour. Res.* **50** (3), 2227–2241.

HILL, K. M., DELLANGELO, L. & MEERSCHAERT, M. M. 2010 Heavy-tailed travel distance in gravel bed transport: an exploratory enquiry. *J. Geophys. Res.* **115** (F2), F00A14.

KASPRAK, A., WHEATON, J. M., ASHMORE, P. E., HENSLEIGH, J. W. & PEIRCE, S. 2015 The relationship between particle travel distance and channel morphology: results from physical models of braided rivers. *J. Geophys. Res.* **120** (1), 55–74.

LAJEUNESSE, E., MALVERTI, L. & CHARRU, FÇO 2010 Bed load transport in turbulent flow at the grain scale: experiments and modeling. *J. Geophys. Res.* **115** (F4), F04001.

LEE, H-Y., LIN, Y-T., YUNYOU, J. & WENWANG, H. 2006 On three-dimensional continuous saltating process of sediment particles near the channel bed. *J. Hydraul Res.* **44** (3), 374–389.

MARTIN, R. L., JEROLMACK, D. J. & SCHUMER, R. 2012 The physical basis for anomalous diffusion in bed load transport. *J. Geophys. Res.* **117** (F1), F01018.

MCNAMARA, J. P. & BORDEN, C. 2004 Observations on the movement of coarse gravel using implanted motion-sensing radio transmitters. *Hydrol. Process.* **18** (10), 1871–1884.

NIÑO, Y. & GARCIA, M. H. 1996 Experiments on particle-turbulence interactions in the near-wall region of an open channel flow: implications for sediment transport. *J. Fluid Mech.* **326**, 285–319.

NIKORA, V., HABERSACK, H., HUBER, T. & MCEWAN, I. 2002 On bed particle diffusion in gravel bed flows under weak bed load transport. *Water Resour. Res.* **38** (6), 17-1–17-9.

OURIEMI, M., AUSSILLOUS, P. & GUAZZELLI, E. 2009 Sediment dynamics. Part 1. Bed-load transport by laminar shearing flows. *J. Fluid Mech.* **636**, 295–319.

PÄHTZ, T. & DURÁN, O. 2018 The cessation threshold of nonsuspended sediment transport across aeolian and fluvial environments. *J. Geophys. Res.* **123** (8), 1638–1666.

PAINTAL, A. S. 1971 A stochastic model of bed load transport. *J. Hydraul Res.* **9** (4), 527–554.

PYRCE, R. S. & ASHMORE, P. E. 2003 The relation between particle path length distributions and channel morphology in gravel-bed streams: a synthesis. *Geomorphology* **56** (1–2), 167–187.

SÉCHET, P. & LE GUENNEC, B. 1999 Bursting phenomenon and incipient motion of solid particles in bed-load transport. *J. Hydraul Res.* **37** (5), 683–696.

SEIZILLES, G., LAJEUNESSE, E., DEVAUCHELLE, O. & BAK, M. 2014 Cross-stream diffusion in bedload transport. *Phys. Fluids* **26** (1), 013302.

SEMINARA, G., SOLARI, L. & PARKER, G. 2002 Bed load at low shields stress on arbitrarily sloping beds: failure of the bagnold hypothesis. *Water Resour. Res.* **38** (11), 1249.

SHIELDS, A. 1936 Anwendung der Äehnlichkeitsmechanik und der Turbulenzforschung auf die Geschiebebewegung. PhD thesis, Technical University Berlin.

VOEPEL, H., SCHUMER, R. & HASSAN, M. A. 2013 Sediment residence time distributions: theory and application from bed elevation measurements. *J. Geophys. Res.* **118** (4), 2557–2567.

WONG, M. & PARKER, G. 2006 Reanalysis and correction of bed-load relation of Meyer–Peter and Müller using their own database. *J. Hydraul. Engng* **132** (11), 1159–1168.

https://doi.org/10.1017/jfm.2019.563 Published online by Cambridge University Press